

## CHANDRA LETG OBSERVATIONS OF SUPERNOVA REMNANT 1987A

SVETOZAR A. ZHEKOV,<sup>1,2</sup> RICHARD McCRAY,<sup>1</sup> KAZIMIERZ J. BORKOWSKI,<sup>3</sup> DAVID N. BURROWS,<sup>4</sup> AND SANGWOOK PARK<sup>4</sup>

Received 2006 January 25; accepted 2006 March 9

### ABSTRACT

We discuss the results from deep *Chandra* LETG observations of the supernova remnant 1987A (SNR 1987A). We find that a distribution of shocks, spanning the same range of velocities (from  $\sim 300$  to  $1700 \text{ km s}^{-1}$ ) as deduced in the first part of our analysis, can account for the entire X-ray spectrum of this object. The postshock temperature distribution is *bimodal*, peaking at  $kT \sim 0.5$  and  $\sim 3$  keV. Abundances inferred from the X-ray spectrum have values similar to those for the inner circumstellar ring, except that the abundances of nitrogen and oxygen are approximately a factor of 2 lower than those inferred from the optical/UV spectrum. The velocity of the X-ray-emitting plasma has decreased since 1999, apparently because the blast wave has entered the main body of the inner circumstellar ring.

*Subject headings:* supernova remnants — supernovae: individual (SNR 1987A) — X-rays: ISM

### 1. INTRODUCTION

With the rapidly developing impact of the debris of supernova 1987A, with its inner circumstellar ring, we have an unprecedented opportunity to witness the birth of a supernova remnant, SNR 1987A (McCray 2005). The reappearance of SNR 1987A in radio (Staveley-Smith et al. 1992, 1993) and in X-rays (Beuermann et al. 1994; Gorenstein et al. 1994; Hasinger et al. 1996) at  $\sim 1200$  days after the explosion was the first clear sign of this phenomenon. The presence of a triple ring system of relatively dense circumstellar matter (CSM) centered on the supernova (Burrows et al. 1995) ensures that astronomers will be able to follow this exciting event for a long time. Indeed, we see the continuous brightening in radio (Gaensler et al. 1997; Manchester et al. 2002) and X-rays (Park et al. 2004, 2005) as well as the appearance in the optical and ultraviolet (UV) of several rapidly brightening spatially unresolved hot spots (Lawrence et al. 2000; Michael et al. 2000), which by now encircle the entire inner ring (Sugerman et al. 2002).

The hydrodynamics of the interaction of the supernova debris with its circumstellar matter is quite complex (Chevalier et al. 1992; Borkowski et al. 1997a, 1997b), and it depends on the details of the density distribution of the CSM as well as the density and velocity distributions in the supernova debris. In general, a double shock structure forms. The forward shock (blast wave) propagates into the CSM, while a reverse shock propagates backward into the supernova debris. Typically, the separation between the blast wave and the reverse shock is  $\sim 10\%$  of the radius of the blast wave (Chevalier 1982). Between these two shocks are layers of shocked CSM and shocked supernova debris, separated by a (usually unstable) contact discontinuity. These layers are sources of X-ray emission.

Hydrodynamic simulations show that, during the first decades of the supernova remnant evolution, the total soft X-ray emission will be dominated by the shocked CSM behind the blast wave

(Borkowski et al. 1997a). Then, when the blast wave strikes regions of dense gas in the inner circumstellar ring, slower shocks will be transmitted into the ring, while reflected shocks will propagate backward through the shocked CSM and will eventually merge with the reverse shock. This interaction will further enhance the X-ray emission. By analyzing the evolution of the X-ray spectrum of SNR 1987A, we have a unique opportunity to learn about the density distribution and elemental abundances of the supernova CSM, as well as the physics of high-velocity shocks in rarefied gases. These studies may also provide vital clues to the origin of the inner ring.

Continuous monitoring of *Chandra* images of SNR 1987A (e.g., Burrows et al. 2000; Park et al. 2002, 2004, 2005, 2006) have provided us with much information about the evolution of the spatial and thermal distribution of the shocked gas. However, the poor spectral resolution of the CCD data do not allow us to study the kinematics of the X-ray-emitting gas in detail. Such information can be obtained only by analyzing high-resolution dispersed X-ray spectra.

The first dispersed X-ray spectrum of SNR 1987A, obtained in 1999 October with the *Chandra* HETG, was discussed by Michael et al. (2002). Unfortunately, the limited photon statistics only allowed these authors to construct a composite line profile. The  $\sim 5000 \text{ km s}^{-1}$  FWHM of this profile indicated a blast wave (forward shock) velocity  $\sim 3500 \text{ km s}^{-1}$ . When we obtained new *Chandra* (LETG) observations in 2004 September, we expected to see comparable kinematic velocities; but we were surprised to find that the X-ray emission lines had considerably smaller intrinsic widths ( $\sim 500\text{--}1000 \text{ km s}^{-1}$ ). This observation showed clearly that the X-ray emission is now dominated by gas behind shocks of much lower velocities than before (Zhekov et al. 2005, hereafter Paper I).

In Paper I, we measured the widths, line shifts, and fluxes of the strong emission lines from hydrogen- and helium-like ions of abundant chemical elements in the spectral energy range from 0.4 to 3 keV. (At higher energies the spectrum is dominated by continuum emission.) We inferred that the X-ray emission from this object is likely to originate from a distribution of shocks with velocities in the range  $300\text{--}1700 \text{ km s}^{-1}$ . We proposed that this ensemble of shocks is a consequence of the blast wave interaction with the complex density distribution of the inner circumstellar ring, where transmitted as well as reflected shocks play a major role.

In this, the second part of our analysis of the *Chandra* LETG observations, we test these conclusions further by carrying out a

<sup>1</sup> JILA, University of Colorado, Boulder, CO 80309-0440; zhekovs@colorado.edu, dick@jila.colorado.edu.

<sup>2</sup> Current address: Space Research Institute, 6 Moskovska Str., Sofia 1000, Bulgaria.

<sup>3</sup> Department of Physics, North Carolina State University, Raleigh, NC 27695-8202; kborkow@unity.ncsu.edu.

<sup>4</sup> Department of Astronomy and Astrophysics, Pennsylvania State University, 525 Davey Laboratory, University Park, PA 16802; burrows@astro.psu.edu, park@astro.psu.edu.

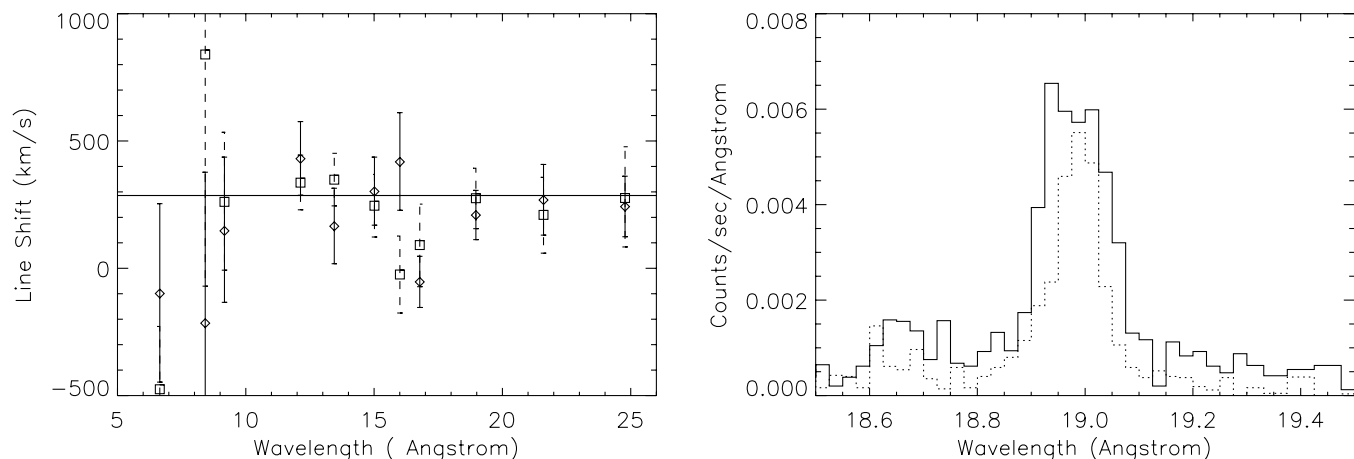


Fig. 1.—*Left*: Line shifts for the strong emission lines in the positive (*diamonds*) and negative (*squares*) LETG first-order spectra of SN 1987A. The solid line in the left panel represents the average redshift for the Large Magellanic Cloud ( $z = 9.53 \times 10^{-4}$ ). *Right*: The O VIII Ly $\alpha$  profile in the positive (*solid line*) and negative (*dashed line*) LETG first-order spectra. The count rate in the  $m = -1$  spectrum has been multiplied by a factor 1.5 to correct for the lower sensitivity of the detector in that arm.

“global” analysis. In § 2 we briefly review our observations and data reduction procedures. In § 3 we summarize the properties of strong X-ray emission lines as described in Paper I. Then in §§ 4 and 5 we analyze the entire LETG spectrum of SNR 1987A and construct a model to fit it. Finally, in § 6 we discuss what our observations imply about the overall picture of the newborn supernova remnant SNR 1987A and its future evolution.

## 2. OBSERVATIONS AND DATA REDUCTION

SNR 1987A was observed with *Chandra* in the configuration LETG-ACIS-S in five consecutive runs (*Chandra* ObsIDs 4640, 4641, 5362, 5363, and 6099) in the period 2004 August 26–September 5 ( $\sim 6398$  days after the explosion), providing a total effective exposure of 289 ks. The roll angle was chosen so that the negative arm of the dispersion axis was aligned approximately north, within  $\sim 15^\circ$  from north to west, thus within  $\sim 10^\circ$  of the minor axis of the inner circumstellar ring (P.A.  $\approx 354^\circ$ ; Sugerman et al. 2002).

We extracted positive ( $m = +1$ ) and negative ( $m = -1$ ) first-order LETG spectra for each of the five observations according to the procedure described in the Science Threads for Grating Spectroscopy in the CIAO 3.1<sup>5</sup> data analysis software. We merged the resulting spectra into one spectrum each for the positive and negative LETG arms, with respective total counts of 9241 and 6057 in the energy range 0.4–7 keV. The difference in photon statistics is a result of the different sensitivities of the respective CCD detectors. For each of the five data sets we extracted a pulse-height spectrum from the zeroth-order image (according to CIAO Science Threads for Image Spectroscopy), contained in a circular region with a radius of 10 pixels centered on the source position. We measured the corresponding background spectrum from an annulus with inner and outer radii of 10 and 20 pixels, respectively. After combining the five pulse-height spectra into one, we measure a total of 16,557 counts in the 0.4–7 keV range. We generated the ancillary response functions for all LETG spectra (first and zeroth order) using the *Chandra* calibration database CALDB v3.00.

## 3. SPECTRAL LINES

Here we summarize the basic results from our analysis in Paper I of the strong X-ray emission lines in the spectrum. We

found that the line profiles had no apparent asymmetries and that the centroids for the emission lines were consistent with the redshift for the Large Magellanic Cloud (see also Fig. 1). Therefore, we could find satisfactory Gaussian fits to the line profiles.

All the lines seen in ( $m = -1$ ) LETG spectrum have smaller widths than their counterparts in the ( $m = +1$ ) spectrum. As described in Paper I, this phenomenon results from the convolution of the spatial structure and velocity gradients in the X-ray source.<sup>6</sup> It is a consequence of the facts that the X-ray source is resolved and that the X-ray-emitting plasma is confined in the plane of an expanding ring. Having anticipated this physical picture and in order to use this effect to maximum advantage, we chose the roll angle for the LETG observations to coincide nearly with the minor axis of the inner circumstellar ring.

## 4. GLOBAL SPECTRAL FITS

A systematic approach to modeling the X-ray spectrum of SNR 1987A would be to make a global fit of the entire observed spectrum using a model consisting of a distribution of shock velocities and ages. Such a global fit has significant advantages over the line ratio analysis presented in Paper I: (1) the fit can automatically take into account the quasi-continuum due to numerous weak lines; (2) by fitting the shape of the underlying continuum (free-free, recombination, and two-photon emission) the model places additional constraints on the plasma temperature; (3) the model can constrain the column density of X-ray absorbing gas; and (4) it can yield estimates of relative element abundances.

It is prohibitive, however, to explore the entire range of models defined by such a continuum in parameter space. Instead, we begin by exploring fits to the spectrum with a model consisting of one or two plane-parallel shocks and then consider a more complex distribution of shocks.

In adopting this approach, we have used the recent version (11.3.2) of the XSPEC code for modeling X-ray emission spectra of shocks. Specifically, we employ the *vpshock* model, which takes into account the nonequilibrium ionization in hot plasmas from version 2.0 of NEI models in XSPEC, which are based on ATOMDB (Smith et al. 2001). We augmented this atomic database by adding inner-shell processes, which are missing in

<sup>5</sup> Chandra Interactive Analysis of Observations (CIAO), <http://cxc.harvard.edu/ciao/>.

<sup>6</sup> This effect is also discussed in The *Chandra* Proposer’s Observatory Guide, Version 7.0, § 8.5.3, pp. 187–189, § 9.3.3, pp. 209–215.

TABLE 1  
SHOCK FITTING RESULTS (FIRST- AND ZEROth-ORDER SPECTRA)

PARAMETER	LETG FIRST-ORDER		LETG ZEROth-ORDER
	One Shock	Two Shock	Two Shock
$\chi^2/\text{dof}$ .....	661/436	417/433	121/111
$N_{\text{H}}$ ( $10^{21} \text{ cm}^{-2}$ ).....	0.63 [0.45–0.82]	1.47 [1.25–1.73]	2.13 [1.52–3.00]
$kT_1$ (keV).....		0.50 [0.47–0.54]	0.41 [0.35–0.66]
$kT_2$ (keV).....	2.16 [2.08–2.21]	2.72 [2.44–3.02]	3.40 [2.63–4.06]
$\tau_1^{\text{a}}$ .....		5.21 [3.73–7.83]	6.36 [3.10–29.1]
$\tau_2^{\text{a}}$ .....	0.69 [0.62–0.77]	1.43 [0.77–15.4]	1.43 [0.76–13.5]
$\text{EM}_1^{\text{b}}$ .....		5.51	12.7
$\text{EM}_2^{\text{b}}$ .....	2.45	1.69	1.44
H.....	1	1	1
He (2.57).....	2.57	2.57	2.57
C (0.09).....	0.09	0.09	0.09
N (1.63).....	0.40 [0.32–0.50]	0.77 [0.60–1.00]	0.12 [0.0–0.73]
O (0.18).....	0.055 [0.047–0.066]	0.092 [0.075–0.104]	0.10 [0.073–0.15]
Ne (0.29).....	0.25 [0.22–0.28]	0.29 [0.25–0.34]	0.29 [0.21–0.41]
Mg (0.32).....	0.21 [0.18–0.24]	0.24 [0.20–0.28]	0.23 [0.16–0.33]
Si (0.31).....	0.24 [0.21–0.27]	0.28 [0.22–0.32]	0.66 [0.47–1.12]
S (0.36).....	0.42 [0.28–0.56]	0.45 [0.32–0.60]	0.43 [0.24–0.96]
Ar (0.54).....	0.54	0.54	0.54
Ca (0.34).....	0.34	0.34	0.34
Fe (0.22).....	0.16 [0.14–0.18]	0.16 [0.14–0.17]	0.11 [0.08–0.18]
Ni (0.62).....	0.62	0.62	0.62
$F_{\text{X}}$ (0.5–2 keV) <sup>c</sup> .....	1.42	1.47	1.55
$F_{\text{X}}$ (0.5–6 keV) <sup>c</sup> .....	1.80	1.84	1.95

NOTE.—90% confidence intervals are given in brackets, and all abundances are expressed as ratios to their solar values (Anders & Grevesse 1989). For comparison, the inner-ring abundances of He, C, N, and O (Lundqvist & Fransson 1996); those of Ne, Mg, Si, S, and Fe typical for the LMC SNRs (Hughes et al. 1998); and Ar, Ca and Ni abundances representative for LMC (Russell & Dopita 1992) are given in the first column in parentheses. Note that the H, He, C, Ar, Ca, and Ni abundances were kept fixed in all model fits (see text).

<sup>a</sup> ( $n_e t$ ) in units of  $10^{11} \text{ s cm}^{-3}$ .

<sup>b</sup>  $\text{EM} = \int n_e n_{\text{H}} dV$  in units of  $10^{58} \text{ cm}^{-3}$ , assuming a distance of 50 kpc.

<sup>c</sup> X-ray flux in units of  $10^{-12} \text{ ergs cm}^{-2} \text{ s}^{-1}$ .

NEI v2.0. In such shock models, the X-ray emission properties are functions of the postshock temperature and the ionization age,  $n_e t$ , defined as the product of the postshock electron density and the time since the gas first entered the shock. Details of these models are found in Borkowski et al. (2001).

To determine the elemental abundances in our fits, we adopted the same procedure as in our previous spectral analyses (Michael et al. 2002; Park et al. 2002, 2004). That is, we only varied the abundances of elements having strong emission lines in the observed (0.5–4 keV) energy range, namely, N, O, Ne, Mg, Si, S, and Fe. We fixed the abundances of He and C to the values determined by Lundqvist & Fransson (1996) from fits to the optical/UV spectrum of the inner ring and the abundances of the remaining elements (Ar, Ca, and Ni) to values representative of the Large Magellanic Cloud (Russell & Dopita 1992).

We fitted the positive ( $m = +1$ ) and negative ( $m = -1$ ) LETG first-order spectra simultaneously with models having identical plasma characteristics but different line broadening parameters, defined as in Paper I. Namely, we assumed that the line profiles are Gaussian with three sources of line broadening: (1) the spatial extent of the image itself, which can be expressed as an equivalent line broadening, independent of wavelength; (2) the thermal broadening of the shocked gas; and (3) the broadening due to the bulk motion of the shocked gas. For plasma temperatures of interest here ( $kT \approx 0.1$ –4 keV) the thermal line broadening for heavy elements (N through Fe) is negligible compared to the other two sources. This is because the standard relations between the shock parameters yield a ratio of the ion thermal velocity to the

postshock bulk gas velocity,  $V_{\text{th}}/V_{\text{bulk}} = [(2/3)(\mu/A)]^{1/2} = 0.7/A^{1/2}$ , where the mean particle weight  $\mu = 0.72$  for SNR 1987A, and  $A$  is the mass of a given ion in units of the proton mass. Therefore, the thermal velocity of various ionic species is only between 10% and 20% of the bulk gas velocity ( $A = 14$  [N] through 56 [Fe]). On the other hand, the spatial size of SNR 1987A in wavelength units ( $\Delta\lambda_0 = 0.047 \text{ \AA}$ ; Paper I) results in a line broadening larger than that from the bulk gas velocity of the shocked gas. Therefore, we express the net line width (FWHM) as

$$\Delta\lambda_{\text{tot}} = 2\Delta\lambda_0 \pm 2z_0(\lambda/\lambda_0)^\alpha \lambda, \quad (1)$$

where the plus (minus) sign refers to the  $m = +1$  ( $m = -1$ ) spectrum, respectively. The first term on the right-hand side of equation (1) represents the broadening due to the spatial extent of the source. The second term represents the broadening due to the bulk motion. The power-law function of wavelength in the second term allows for the possibility that the mean bulk velocity of shocked gas emitting a given line may depend on the excitation or ionization stage of the emitting ion. The parameter  $z_0$  determines the line broadening at some fiducial wavelength,  $\lambda_0$ , and the power-law index  $\alpha$  is to be determined.

#### 4.1. Discrete Shock Models

We fitted one- and two-shock models to the LETG spectra of SNR 1987A (rebinned to have a minimum of 30 counts per bin). The results from our model fits are shown in Table 1. We find that a fit with a one-shock model is statistically unacceptable and that

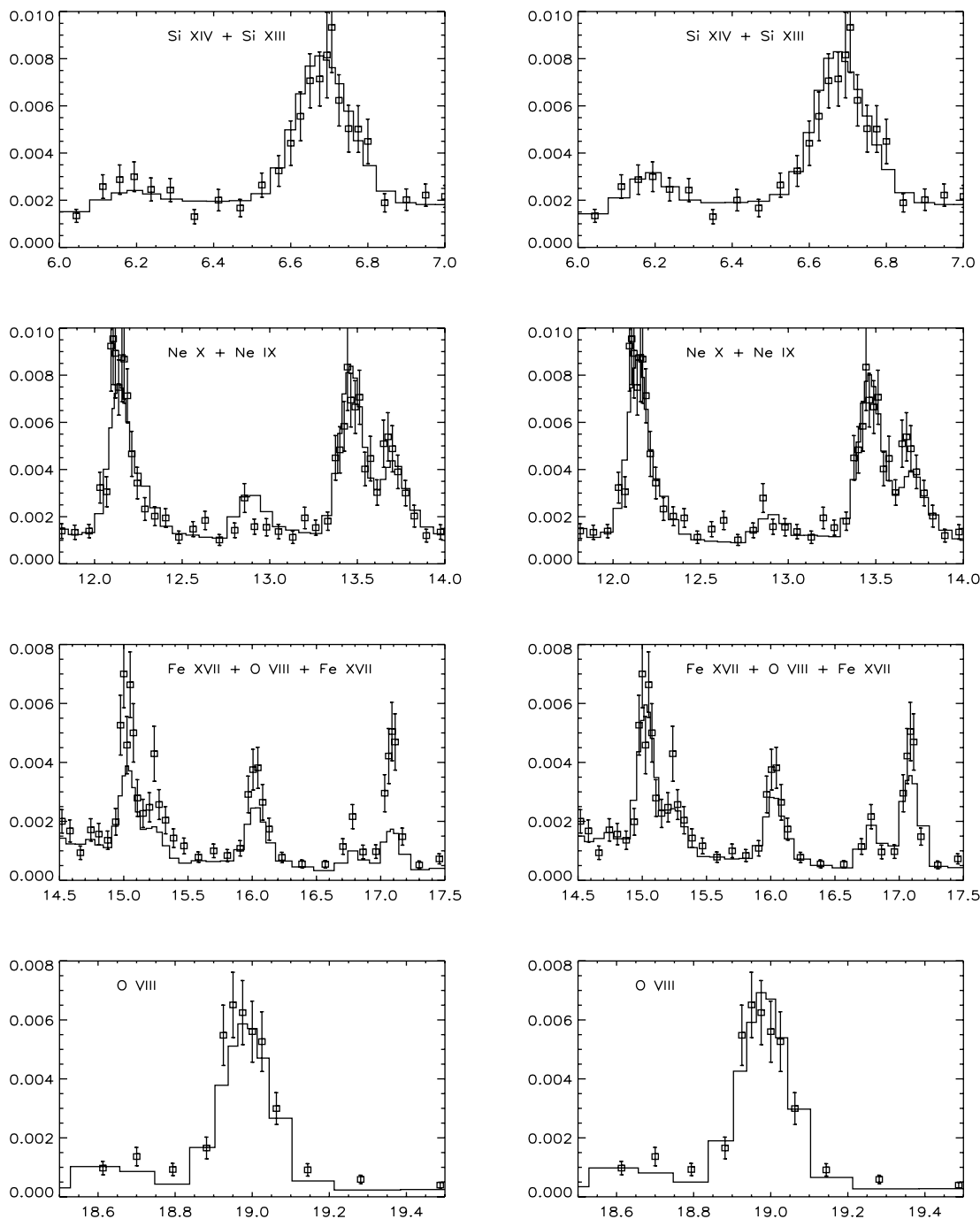


FIG. 2.—Positive first-order LETG X-ray spectrum of SNR 1987A (rebinned to have a minimum of 30 counts  $\text{bin}^{-1}$  near some strong spectral lines). Open squares with  $1\sigma$  error bars show the observed spectrum; solid line shows fits from the XSPEC one-shock (*left column*) and two-shock (*right column*) models (see Table 1). Horizontal axes are the observed wavelength ( $\text{\AA}$ ); vertical axes are the flux density ( $\text{photons s}^{-1} \text{\AA}^{-1}$ ).

it yields an unreasonably small X-ray absorption column density. (This value is from 3 to 4 times smaller than that derived from the previous X-ray observations [Michael et al. 2002; Park et al. 2004], whose results were consistent with the neutral hydrogen column density toward SNR 1987A deduced from observations in the optical and UV [Fitzpatrick & Walborn 1990; Scuderi et al. 1996]). Figure 2 also illustrates how difficult it is for the one-shock model to give a good fit to spectral lines of ionic species that require different plasma conditions (e.g., Si XIII and Si XIV with ionization potential [IP] of 2.67 and 2.44 keV, and Fe XVII with IP of 1.27 keV). Therefore, we favor the two-shock model. The results for the line broadening from the global fit are

close to those derived in Paper I:  $z_0 = 1.13 \times 10^{-3}$  [ $7.4 \times 10^{-4} - 1.54 \times 10^{-3}$ ] versus  $1.57 \times 10^{-3}$ ;  $\lambda_0 = 0.061$  [0.057 to 0.064] versus 0.047  $\text{\AA}$ ; and  $\alpha = -1.17$  [ $-1.94$  to  $-0.08$ ] versus  $-1.3$  (the 90% confidence limits are given in brackets). The relatively small differences can be attributed to the fact that the global fitting procedure simultaneously handles both lines and continuum.

As a check, we also fitted one- and two-shock models to the pulse-height spectrum of the zeroth-order LETG image. The best-fit (two-shock) results are shown in Table 1. Of course, the parameters determined from the pulse-height spectrum, especially the abundances, are less tightly constrained than those determined from the dispersed images. However, agreement of the fit to the

pulse-height spectrum with the fit to the dispersed spectrum gives us confidence in also using the pulse-height spectrum to infer element abundances and conditions in the X-ray emitting gas.

The abundances of SNR 1987A derived here are consistent with those derived from previous CCD spectra (Michael et al. 2002; Park et al. 2004). We find that the abundances of Ne, Mg, Si, S, and Fe are very close to those found in X-rays for the LMC SNRs (Hughes et al. 1998). On the other hand, the N and O abundances derived here are lower by a factor of about 2 than those found for the inner ring by Lundqvist & Fransson (1996). We note that similar lower nitrogen abundance was found by Pun et al. (2002) in their analysis of the optical and UV spectrum of spot 1 on the inner circumstellar ring. But it is interesting to note that the relative abundance of nitrogen and oxygen derived in our analysis,  $N/O = 1.1$  (by number), is consistent with that derived from the modeling of the optical/UV emission of the inner ring (Lundqvist & Fransson 1996; Sonneborn et al. 1997). Thus, we confirm the nitrogen enhancement in the CSM around SNR 1987A, which strongly suggests that the CSM consists of matter that had undergone CNO processing in progenitor star and was subsequently ejected.

Significant departures from electron-ion temperature equilibration may be present in the postshock plasma (Michael et al. 2002). In the fits we present here, we have not included this effect. We have explored models including departures from electron-ion temperature equilibration (the `vpshock` option in XSPEC), and we find that they give equally good fits to the spectra, but a detailed analysis of such models is beyond the scope of this paper (see also § 6).

#### 4.2. Distribution of Shocks

One of the basic results from the line-profile analysis of Paper I was that a distribution of shocks with velocities in the range  $340\text{--}1700\text{ km s}^{-1}$  is compatible with the LETG data. Given the relation between the postshock temperature and the shock velocity for strong adiabatic shocks with electron-ion temperature equilibration,

$$kT_e = \frac{3}{16} \mu V_S^2 = 1.4 (V_S/1000\text{ km s}^{-1})^2\text{ keV}, \quad (2)$$

where  $\mu = 0.72m_p$  for SNR 1987A. The observed velocity range corresponds to a temperature range of  $kT_e = 0.15\text{--}4\text{ keV}$ .

To develop this scenario, we constructed a new XSPEC model having the following features: (1) the distribution of emission measures in the shocked gas is determined from the Chebyshev polynomial algorithm as is used in the standard XSPEC `c6pvmk1` model (Lemen et al. 1989); (2) the basis vectors for X-ray emission from the distribution of shocks are those from the XSPEC `vpshock` model; and (3) all shocks share the same element abundances and X-ray absorption. Moreover, to decrease the number of free parameters, we also assumed that (4) the ionization age ( $n_e t$ )<sub>*i*</sub> of each individual shock *i* is a power-law function of the postshock temperature, i.e.,  $(n_e t)_i \propto (kT_e)_i^p$ , where *p* is a free parameter. Details of the line broadening are given below.

As in our earlier analysis, we assume the emission lines to be Gaussian profiles with FWHM depending on the wavelength. We recall that the wavelength dependence of the line width represents the physical notion that faster shocks produce higher temperature plasma, whose emission is dominated by lines at shorter wavelengths. Now, by fitting the entire spectrum with models having a distribution of shock velocities, we can test this assumption in a more rigorous way. Namely, we assume that the total X-ray spectrum of a parcel of shocked plasma (having

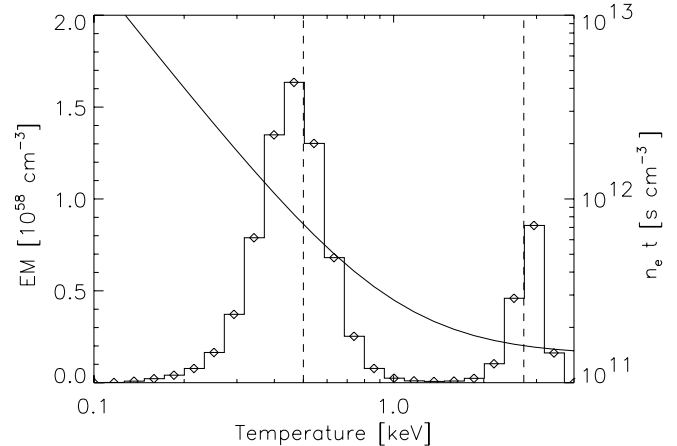


Fig. 3.—Emission measure (EM) distribution of shocks in SNR 1987A as derived from the DS model with 25 points logarithmically spaced in the (0.1–4 keV) postshock temperature range. The two vertical dashed lines indicate the plasma temperature derived from the discrete two-shock model. The solid line shows the derived ionization age of each shock ( $n_e t$ ).

temperature  $T_e$ ) is moving with postshock velocity given by equation (2). Then, similarly to equation (1) we write

$$\Delta\lambda_{\text{tot}} = 2\Delta\lambda_0 \pm 2z_S\lambda, \quad (3)$$

where  $z_S = \beta(3/4)V_S/c$ ,  $V_S$  is the shock velocity,  $3/4$  stands for the case of a strong shock entering a stationary gas, and  $c$  is the speed of light. The parameter  $\beta$  ( $0 \leq \beta \leq 1$ ) allows for various geometrical effects, such as viewing angle, to be considered as well.

With these assumptions, we can find a satisfactory ( $\chi^2/\text{dof} = 414/431$ ) simultaneous fit to the positive and negative LETG spectra of SNR 1987A. Figure 3 shows the distribution function of emission measures and ionization ages determined by the fit. Note that the shape of the inferred shock distribution is *bimodal*, peaking very close to the temperature values derived in our discrete two-shock model fit. To verify this conclusion, we tried to fit various models having more X-ray plasma with temperature between the two peaks. In no case could we find an acceptable fit without a bimodal distribution. Note also that the ionization age of the shocked gas decreases with increasing shock temperature.

The absorption column density and element abundances have the values (with  $1\sigma$  errors)  $N_H = 1.52 \pm 0.02 \times 10^{21}\text{ cm}^{-2}$ ,  $N = 0.88 \pm 0.13$ ,  $O = 0.10 \pm 0.01$ ,  $Ne = 0.31 \pm 0.02$ ,  $Mg = 0.25 \pm 0.02$ ,  $Si = 0.29 \pm 0.02$ ,  $S = 0.48 \pm 0.09$ , and  $Fe = 0.16 \pm 0.02$ . We note that these parameters are also very close to those determined from the two-shock model fit (for comparison see Table 1). Moreover, the derived value of  $\beta = 0.35 \pm 0.06$  is close to that expected for a radial gas motion in a disk viewed at inclination angle  $i$ ,  $\overline{\sin\phi \sin i} = 0.45$  ( $\overline{\sin\phi} = 2/\pi$ ,  $0 \leq \phi \leq \pi/2$ ;  $i = 45^\circ$  for the inner ring; Sugerman et al. 2002). These results give us confidence in our global fits to the LETG spectrum of SNR 1987A.

#### 5. MARX SIMULATIONS

As a final test of our model, we used the MARX<sup>7</sup> software to simulate the actual two-dimensional images and dispersed spectra that incorporate the kinematic and spectral information deduced from our analysis of the line profiles, line ratios, and global fits to the observed X-ray spectra of SNR 1987A. Since

<sup>7</sup> See <http://space.mit.edu/CXC/MARX/>.

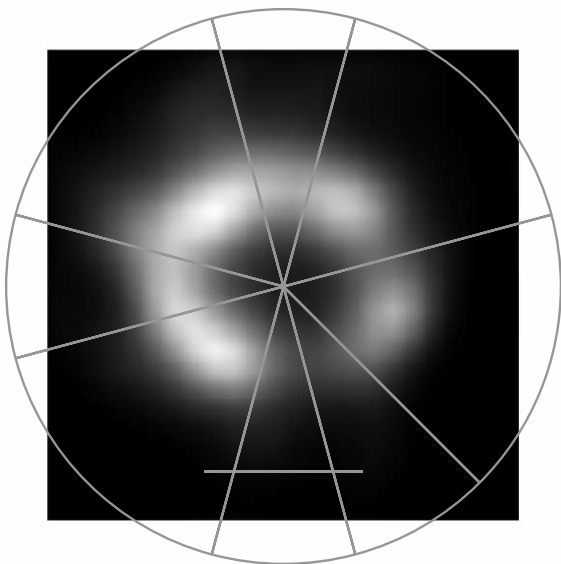


FIG. 4.—Deconvolved zeroth-order image from the LETG observations of SNR 1987A. North is up and east is on the left. Shown are the boundaries of the eight sectors (*subimages*) used in the MARX simulations (§ 5). The horizontal line ( $1''$ ) indicates the scale of the image.

the object is spatially resolved by *Chandra*, our simulations take into account the actual brightness distribution of the X-ray emission as well. The simulations correspond to the actual observing conditions (e.g., date of observation, exposure time, pointing of the telescope, roll angle, etc.).

The actual brightness distribution of the X-ray emission used in our simulations is shown in Figure 4. This is the zeroth-order image from our LETG observations deconvolved according to the same procedures used in our imaging observations (Burrows et al. 2000; Park et al. 2002, 2004). Also shown are the eight sectors we used to represent the details of the image morphology.

To construct the input spectra, we assume that the X-ray-emitting plasma is confined in the plane of the inner ring and that it is expanding radially. Locally, we assume a distribution of shocks with characteristics as described in § 4.2 (see also Fig. 3), with emission measure scaled to correspond to the brightness distribution in each sector.

We constructed our MARX simulations according to the following procedure. For each sector, we simulated the observed spectrum, assuming that the X-ray spectrum corresponds to the physical picture given above and a flux scaled to the total observed flux from SNR 1987A according to the fractional brightness of that sector in the zero-order image. We determined the redshift or blueshift of the spectrum of each sector according to its postshock plasma velocity, corrected for its position (azimuthal angle), and the inclination of the inner ring ( $i = 45^\circ$ ). We then concatenated the resulting simulated data from the all sectors to derive a data set for the entire object. We then extracted the simulated LETG spectra following the CIAO Science Threads for Grating Spectroscopy. In order to minimize the statistical fluctuations in the simulated spectra, we averaged the 10 different realizations of the simulated spectra.

Figures 5, 6, and 7 display these average spectra overlaid with the observed positive and negative first-order LETG spectra. The excellent correspondence between the simulated and actual spectra gives us confidence that our model is a reasonable approximation to the actual interaction of the blast wave with the inner ring.

## 6. DISCUSSION AND CONCLUSIONS

The analysis of the LETG spectra of SNR 1987A presented in §§ 4 and 5 of this paper confirms and refines the main conclusions of Paper I. The X-ray-emitting plasma is largely confined to a radially expanding ring near the inner optical ring. The X-ray-emitting gas is heated by a distribution of shocks and is not in ionization equilibrium. The electron temperature distribution of the shocked gas is bimodal, with peaks at  $\sim 0.5$  and  $\sim 3$  keV.

Our analysis leads us to a general picture of SNR 1987A in which the X-ray emission is dominated by two components. The hot ( $kT_e \sim 3$  keV) component results from shocks of relatively high velocity that propagate through relatively low density ( $n_e \sim 10^2$  cm $^{-3}$ ) circumstellar gas. The cool ( $kT_e \sim 0.5$  keV) component results from shocks transmitted into the denser ( $n_e \sim 10^4$  cm $^{-3}$ ) gas of the inner circumstellar ring.

The fact that the inferred ionization age decreases with shock velocity (Fig. 2) is consistent with this picture. The slower shocks propagate through the higher density gas, while the faster shocks propagate through the lower density gas. Therefore, if the typical timescale since the shock has entered the gas is comparable ( $t \sim$  a few years), the ionization age,  $n_e t$ , of the gas behind the slower shocks will be substantially greater than that of the gas behind the faster shocks.

In their analysis of a spectrum of SNR 1987A taken with the High Energy Transmission Grating of *Chandra* in 1999 October, Michael et al. (2002) inferred an electron temperature  $kT_e \sim 2.6$  keV from the line ratios. By stacking all the emission lines into a composite profile, they also measured the width FWHM  $\approx 5000$  km s $^{-1}$  of a composite line profile, from which they inferred a “typical” shock velocity  $\approx 3500$  km s $^{-1}$  that was consistent with the radial expansion velocity of the X-ray image as measured by Park et al. (2002).

Since the gas behind such a shock would have electron temperature  $\sim 17$  keV if the electrons and ions were in temperature equilibrium, Michael et al. (2002) concluded that the electron and ion temperatures had not equilibrated. This was a reasonable scenario, since the electron-ion temperature equilibration time,  $(n_e t) = 4 \times 10^{11} (kT_{\text{keV}})^{1.5}$  cm $^{-3}$  s (Spitzer 1962), of such a gas would be substantially greater than the typical ionization age,  $n_e t \sim 4 \times 10^{10}$  cm $^{-3}$  s, of shocked gas having  $n_e \approx 400$  cm $^{-3}$  and  $t \sim 3$  yr.

But the shock environment of SNR 1987A has changed considerably since that observation. The line profiles of the current (2004 September) observations (Paper I) indicate shock velocities 300–1700 km s $^{-1}$ , and hence typical postshock temperatures  $kT_e \sim 0.1$ –4 keV. Moreover, such low shock velocities suggest that the shocked gas must have greater density, say,  $4 \times 10^4$  cm $^{-3} > n_e > 1600$  cm $^{-3}$ . From these considerations and Figure 2, we conclude that there is no longer any compelling evidence that the electrons and ions in the shocked gas are out of temperature equilibrium, although this may still be the case for gas behind the faster shocks propagating through the lower density gas.

We expect the rapid evolution of the X-ray spectrum to continue. Park et al. (2005) found that the X-ray light curve is brightening at an accelerating rate. This fact and the correlation of the X-ray image with the optical hot spots (Park et al. 2006) indicate that the blast wave is interacting with much denser gas than in the past. This observation is supported by the noticeable deceleration of the radial expansion velocity of the X-ray image. The most recent *Chandra* data show that this velocity has decreased from  $\sim 4000$  km s $^{-1}$  (Park et al. 2004) to  $\sim 1600$  km s $^{-1}$  (J. Racusin et al. 2006, in preparation).

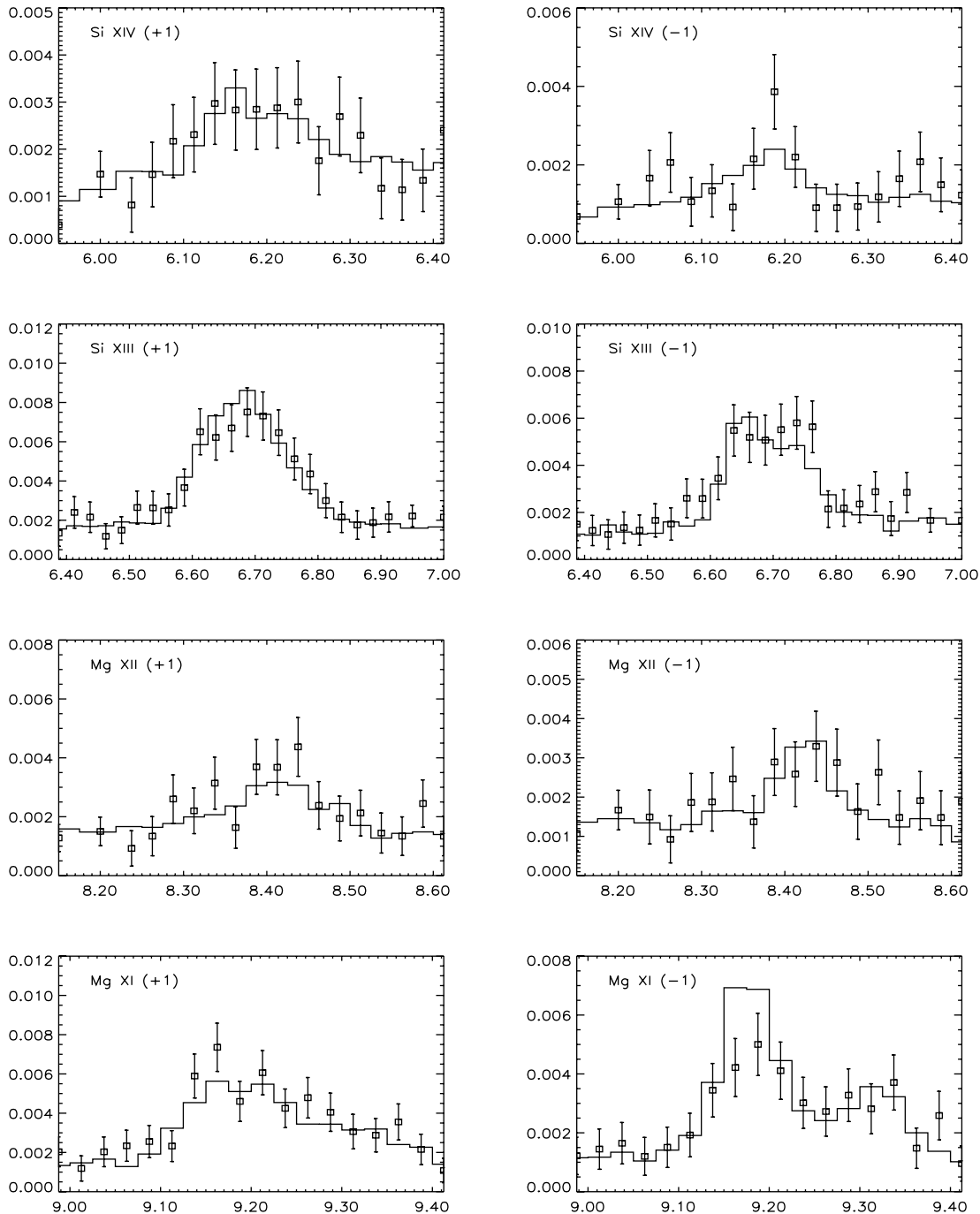


FIG. 5.—X-ray spectrum of SNR 1987A near the strong spectral lines of the H-like and He-like ions Si XIV, Si XIII, Mg XII, and Mg XI. Open squares with  $1\sigma$  error bars show the observed spectrum; solid line shows the simulated MARX spectrum. Horizontal axes are the observed wavelength ( $\text{\AA}$ ); vertical axes are the flux density ( $\text{photons s}^{-1} \text{\AA}^{-1}$ ). The positive and negative first-order LETG spectra are shown in the left and right columns, respectively.

The rapid brightening of the X-ray light curve of SNR 1987A (Park et al. 2005) ensures that we may soon be able to obtain spectra with excellent photon statistics. Thus, with future *Chandra* observations we should be able to constrain the model further and subject it to some critical tests.

When the blast wave strikes dense clumps of gas in the circumstellar ring, the interaction will give rise to both transmitted and reflected shocks, both of which will cause enhanced X-ray emission correlated with the optical hot spots. In both cases the velocity distribution of the shocked gas will shift toward lower velocities. Therefore, we expect that the X-ray emission lines will continue to become narrower.

The evolution of the temperature distribution of the X-ray-emitting gas will tell us the relative contribution of reflected and transmitted shocks to the rapidly brightening source. If the gas behind the transmitted shocks dominates the X-ray emission, the bimodal temperature distribution of the X-ray-emitting gas will become more skewed toward lower temperatures. In fact, Park et al. (2005) have already noticed this trend in their two-shock model fits to *Chandra* nondispersed (ACIS-S) spectra over the past 5 years. On the other hand, if the gas behind the reflected shocks contributes substantially to the X-ray emission, the hot component in the X-ray spectrum will continue to remain substantial.

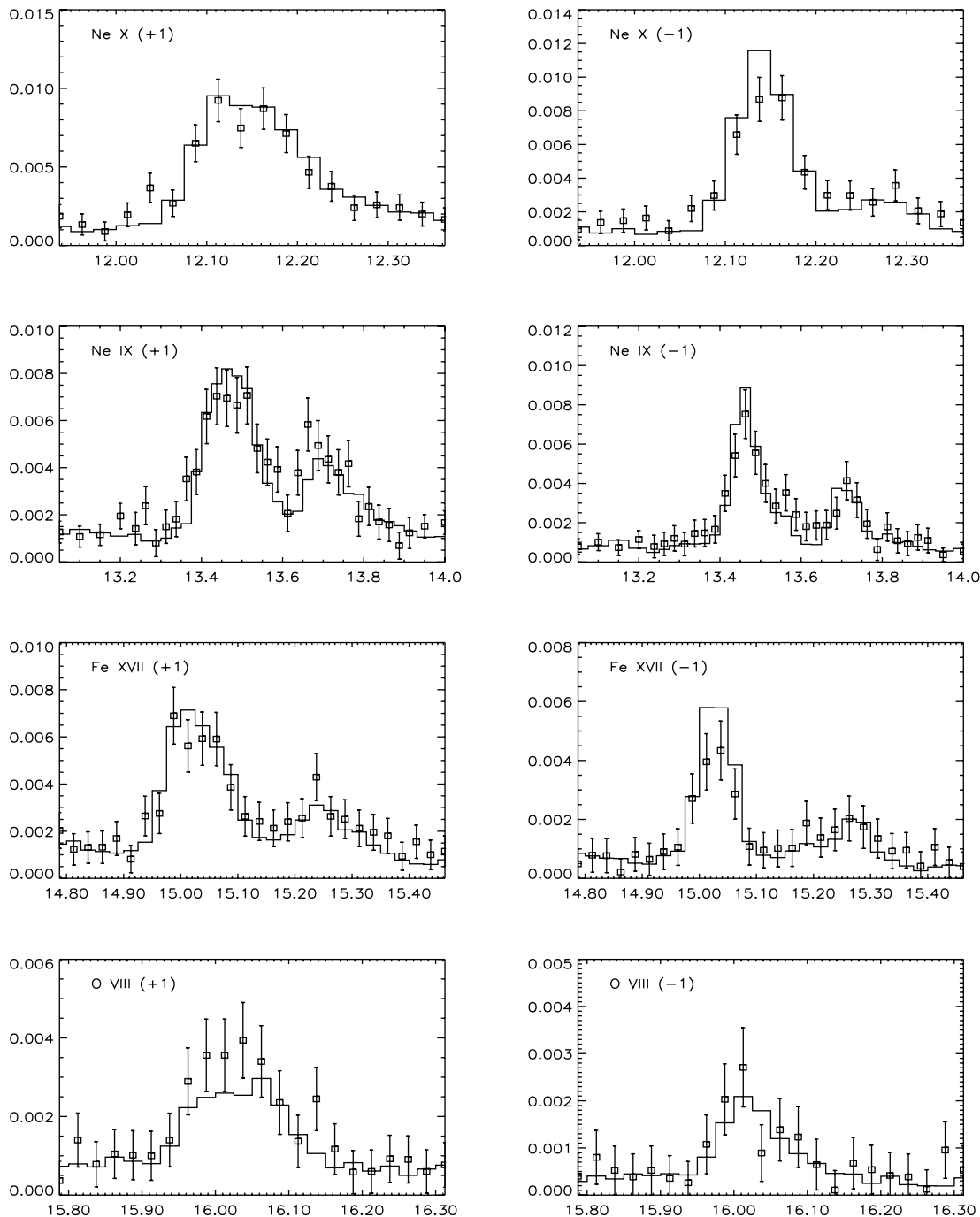


FIG. 6.—As in Fig. 5, but for the H-like and He-like ions of Ne x and Ne ix and the strong lines of Fe xvii and O viii ( $Ly\beta$ ).

The radio emission from SNR 1987A is nonthermal (Gaensler et al. 1997; Manchester et al. 2002) and is probably produced by relativistic electrons accelerated by the reverse shock (Manchester et al. 2005). Park et al. (2005) have noted that the hard X-ray light curve resembles the radio light curve of SNR 1987A and have suggested that the radio emission and the hard X-rays might have a common origin. This suggestion raises the question of whether the X-ray spectrum may have a nonthermal (i.e., power-law) component. Up to now, we have seen no compelling evidence for the presence of such a component, either in the pulse-height spectra (Michael et al. 2002) or in the LETG spectrum discussed here. On the other hand, we cannot rule out the

possibility of a significant nonthermal component, especially at photon energies  $>4$  keV.

Observations of broad line profiles of  $Ly\alpha$  and  $H\alpha$  (Michael et al. 2003; Smith et al. 2005) show that the supernova debris is crossing this reverse shock with velocities  $\sim 10^4$  km s $^{-1}$ . If the hard X-rays originate from the region behind the reverse shock and are produced by thermal processes, then we would expect to see strong emission lines of high-ionization species with relatively broad profiles ( $\sim$  a few  $10^3$  km s $^{-1}$ ). On the other hand, if the hard X-rays are predominantly nonthermal, we would expect to see a decrease in the equivalent widths of the X-ray emission lines at higher energy.

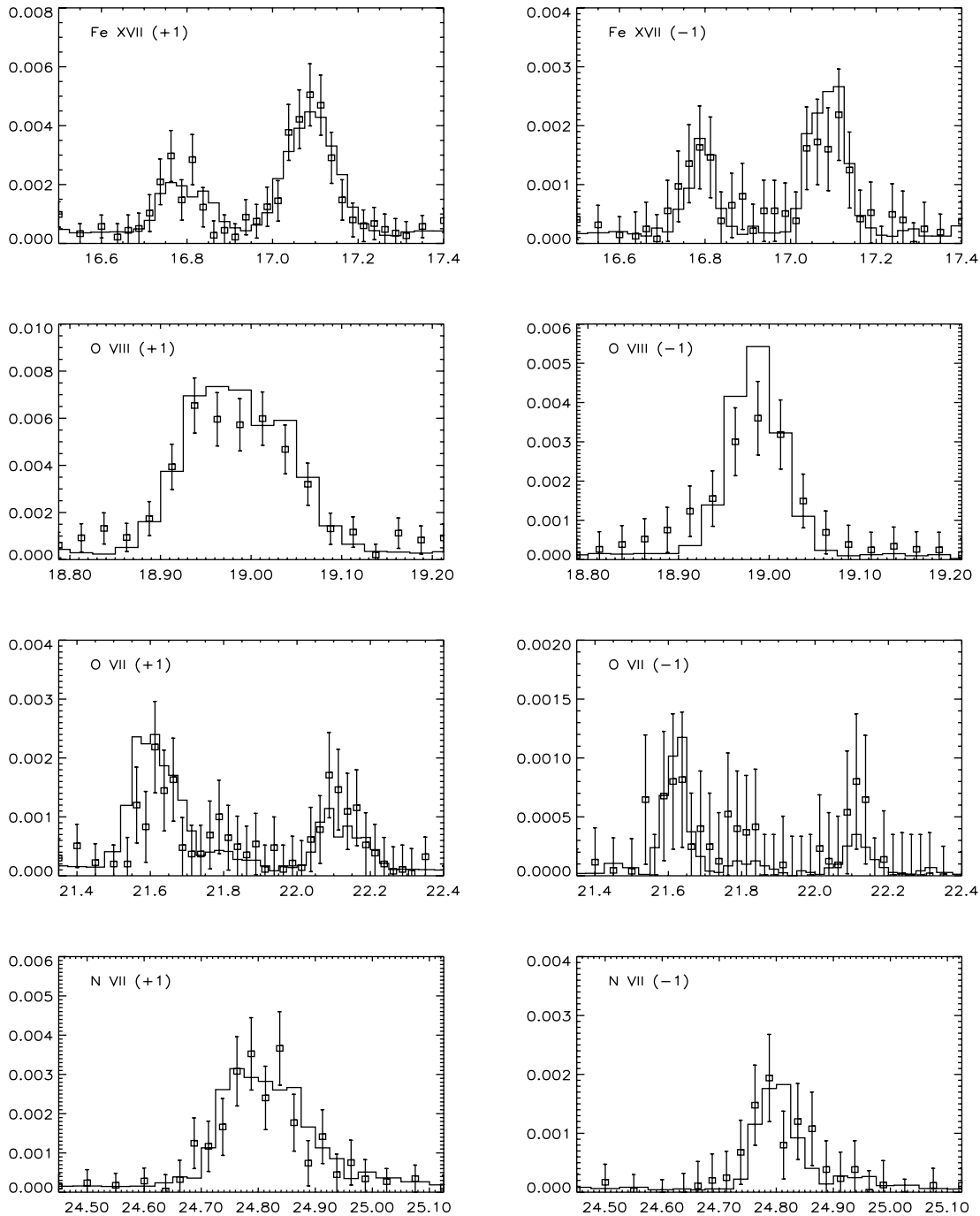


FIG. 7.—As in Fig. 5, but for Fe XVII, the H-like and He-like ions of O VIII ( $\text{Ly}\alpha$ ) and O VII, and the H-like ion of N VII.

Future *Chandra* observations will be also helpful in resolving the issue with the CNO abundances derived in X-rays. As discussed in § 4 (see also Table 1), the N/O ratio is consistent with the value derived from the analysis of the optical/UV spectra of the inner ring in SNR 1987A, but the total amount of light metals (C, N, O) derived in our analysis ( $\text{CNO} \approx 0.15$  solar) is a factor of 2 lower than that derived from optical/UV spectra ( $\text{CNO} \approx 0.28$  solar; see Lundqvist & Fransson 1996). The latter ratio is consistent with the average CNO abundances for LMC ( $\text{CNO} \approx 0.26$  solar; Russel & Dopita 1992). This means that the X-ray analysis confirms the enhancement of the N/O ratio, which may be attributed to CNO processing of the matter by the progenitor

star. But the X-ray observations indicate a deficit in the net abundance of C+N+O (the CNO processing cannot alter their total amount). On the other hand, the abundances of heavier metals (Ne, Mg, Si, S, and Fe) derived here are consistent with typical values for the SNRs in LMC (Hughes et al. 1998).

What could account for the low abundances of C+N+O derived from the X-ray spectrum? On the one hand, we cannot rule out the possibility of purely technical reasons for this discrepancy, such as greater uncertainties in the X-ray spectrum at low energies due to CCD degradation or uncertainties in the atomic data. On the other hand, there might be physical reasons. Could the amount of CNO elements in the progenitor star be considerably

lower (by a factor of 2) than the average for LMC? Or could there be an extra source of (likely nonthermal) continuum, the effect of which would be to reduce the CNO abundances if interpreted as thermal continuum? Future *Chandra* grating observations with anticipated better photon statistics will help us find the correct answer. In addition, such observations may also reveal some evolution (increase) for the abundances of elements like O, Mg, Si, and Fe resulting from the destruction of dust from the supernovae

debris and the inner circumstellar ring by the shocked hot gas emitting in X-rays.

This work was supported by NASA through *Chandra* Awards G04-5072A (to University of Colorado, Boulder) and G04-5072B (to North Carolina State University, Raleigh).

## REFERENCES

- Anders, E., & Grevesse, N. 1989, *Geochim. Cosmochim. Acta*, 53, 197  
 Beuermann, K., Brandt, S., & Pietsch, W. 1994, *A&A*, 281, L45  
 Borkowski, K. J., Blondin, J. M., & McCray, R. 1997a, *ApJ*, 476, L31  
 ———. 1997b, *ApJ*, 477, 281  
 Borkowski, K. J., Lyerly, W. J., & Reynolds, S. P. 2001, *ApJ*, 548, 820  
 Burrows, C. J., Krist, J., Hester, J. J., et al. 1995, *ApJ*, 452, 680  
 Burrows, D. N., et al. 2000, *ApJ*, 543, L149  
 Chevalier, R. A. 1982, *ApJ*, 258, 790  
 Chevalier, R. A., Blondin, J. M., & Emmering, R. T. 1992, *ApJ*, 392, 118  
 Fitzpatrick, E. L., & Walborn, N. L. 1990, *AJ*, 99, 1483  
 Gaensler, B. M., Manchester, R. N., Staveley-Smith, L., Tzioumis, A. K., Reynolds, J. E., & Kesteven, M. J. 1997, *ApJ*, 479, 845  
 Gorenstein, P., Hughes, J. P., & Tucker, W. H. 1994, *ApJ*, 420, L25  
 Hasinger, G., Aschenbach, B., & Trümper, J. 1996, *A&A*, 312, L9  
 Hughes, J. P., Hayashi, I., & Koyama, K. 1998, *ApJ*, 505, 732  
 Lawrence, S. S., Sugerman, B. E., Bouchet, P., Crotts, A. P. S., Uglesich, R., & Heathcote, S. 2000, *ApJ*, 537, L123  
 Lemen, J. R., Mewe, R., Schrijver, C. J., & Fludra, A. 1989, *ApJ*, 341, 474  
 Lundqvist, P., & Fransson, C. 1996, *ApJ*, 464, 924  
 Manchester, R. N., Gaensler, B. M., Staveley-Smith, L., Kesteven, M. J., & Tzioumis, A. K. 2005, *ApJ*, 628, L131  
 Manchester, R. N., Gaensler, B. M., Wheaton, V. C., Staveley-Smith, L., Tzioumis, A. K., Bizunok, N. S., Kesteven, M. J., & Reynolds, J. E. 2002, *Publ. Astron. Soc. Australia*, 19, 207  
 McCray, R. 2005, in *IAU Colloq. 192, Cosmic Explosions*, ed. J. M. Marcaide & K. W. Weiler (Berlin: Springer), 77  
 Michael, E., et al. 2000, *ApJ*, 542, L53  
 Michael, E., et al. 2002, *ApJ*, 574, 166  
 ———. 2003, *ApJ*, 593, 809  
 Park, S., Burrows, D. N., Garmire, G. P., Nousek, J. A., McCray, R., Michael, E., & Zhekov, S. A. 2002, *ApJ*, 567, 314  
 Park, S., Zhekov, S. A., Burrows, D. N., Garmire, G. P., & McCray, R. 2004, *ApJ*, 610, 275  
 Park, S., Zhekov, S. A., Burrows, D. N., Garmire, G. P., Racusin, J. L., & McCray, R. 2006, *ApJ*, in press (astro-ph/0604201)  
 Park, S., Zhekov, S. A., Burrows, D. N., & McCray, R. 2005, *ApJ*, 634, L73  
 Pun, C. S. J., et al. 2002, *ApJ*, 572, 906  
 Russel, S. C., & Dopita, M. A. 1992, *ApJ*, 384, 508  
 Scuderi, S., Panagia, N., Gilmozzi, R., Challis, P. M., & Kirshner, R. P. 1996, *ApJ*, 465, 956  
 Smith, N., Zhekov, S. A., Heng, K., McCray, R., Morse, J. A., & Gladders, M. 2005, *ApJ*, 635, L41  
 Smith, R. K., Brickhouse, N. S., Liedahl, D. A., & Raymond, J. C. 2001, *ApJ*, 556, L91  
 Sonneborn, G., Fransson, C., Lundqvist, P., Cassatella, A., Gilmozzi, R., Kirshner, R. P., Panagia, N., & Wamsteker, W. 1997, *ApJ*, 477, 848  
 Spitzer, L. 1962, *Physics of Fully Ionized Gases* (2nd ed.; New York: Interscience), 135  
 Staveley-Smith et al. 1992, *Nature*, 355, 147  
 ———. 1993, *Nature*, 366, 136  
 Sugerman, B. E. K., Lawrence, S. S., Crotts, A. P. S., Bouchet, P., & Heathcote, S. R. 2002, *ApJ*, 572, 209  
 Zhekov, S. A., McCray, R., Borkowski, K. J., Burrows, D. N., & Park, S. 2005, *ApJ*, 628, L127 (Paper I)